

U-SEANNET: A SIMPLE, EFFICIENT AND APPLIED U-SHAPED NETWORK FOR DIAGNOSING NASAL DISEASES FROM NASAL ENDOSCOPIC IMAGES

Yubiao Yue², Jun Xue³, Haihua Liang¹, Zhenzhang Li^{1,*}

¹College of Mathematics and Systems Science, Guangdong Polytechnic Normal University

²School of Biomedical Engineering, Guangzhou Medical University

³School of Computer Science and Technology, Anhui University

ABSTRACT

Utilizing deep learning (DL) models to improve the early diagnosis of nasal diseases from nasal endoscopic images holds paramount importance. However, the lack of available datasets stymies advancements in this field. Furthermore, existing models fail to strike a good trade-off between model diagnosis performance, model complexity and parameter size, rendering them unsuitable for practical application. To bridge these gaps, we created the first large-scale nasal endoscopy dataset, named 7-NasEID, comprising 11,352 images that span six nasal diseases and normal samples. Building on this, we proposed U-SEANNet, an innovative architecture, underpinned by depth-wise separable convolutions. Additionally, to augment its discernment capabilities for subtle variations in input images, we further proposed the Global-Local Channel Feature Fusion Module, enabling the U-SEANNet to focus salient channel features from both global and local contexts. Notably, U-SEANNet’s parameter size and GFLOPs are only 0.78M and 0.21, respectively. Employing the 7-NasalEID, we conducted the five-fold cross-validation on U-SEANNet, juxtaposing its performance against seventeen renowned architectures. The experimental results suggest U-SEANNet as the state-of-the-art (SOTA) model, achieves an accuracy of 93.58%, sensitivity of 90.17%, and specificity of 91.27%. These findings demonstrate U-SEANNet’s prodigious potential for diagnosing nasal diseases in practical use, providing the development of efficacious nasal diseases diagnosis tools with a new insight.

Index Terms— Nasal Diseases, Deep Learning, Lightweight Network, Feature Fusion

1. INTRODUCTION

Early and accurate diagnosis of nasal diseases is crucial for improving patients’ quality of life and alleviating the burden on the healthcare system[1, 2]. Because this can effectively

assist medical personnel in adopting more appropriate treatment measures, thereby avoiding the use of drugs with side effects and increasing cure rates[3]. In clinical settings, the predominant approach for the early diagnosis of nasal diseases involves physicians utilizing a nasal endoscope to visually inspect the patient’s nasal cavity[4, 5]. However, due to the often very similar symptoms and nasal appearance changes caused by different nasal diseases[6], the accuracy of interpreting nasal endoscopic images heavily depends on whether the expert has rich clinical experience. This directly results in that common people from limited medical resources and economically disadvantaged families struggling to access reliable medical services, often face delay in diagnosis and misdiagnoses and then miss the best treatment opportunities. Therefore, developing a more efficient and affordable tool for early and accurate of nasal diseases holds significant clinical importance.

In recent times, burgeoning evidence demonstrates the high efficiency and economical of deep learning models in the diagnostic analysis of endoscopic images[4, 7, 8, 9, 10], positioning them as a vanguard in medical diagnosis. However, notwithstanding these advancements, glaring lacunae persist in the study of nasal endoscopy. Foremost among these is the dearth of extensive datasets and limited categorizations, rendering it arduous to holistically appraise the efficacy of deep learning models in nasal endoscopic image recognition—this, in turn, attenuates the model’s generalization performance. Furthermore, extant literature predominantly gravitates towards conventional model evaluation metrics, sidelining some determinants: model complexity and parameter size. Practically, these determinants are quintessential, as they gauge a model’s adaptability for integration into a diverse spectrum of computational devices, particularly those constrained by storage space and computational bandwidth, such as smartphones and low-end personal computers.

In this work, we aimed to utilize deep learning model suitable for practical application for early and accurate diagnosis of nasal diseases from nasal endoscopy images. The contributions of our work can be summarized as the following: (1) we created 7-NasEID, the first large-scale nasal en-

This work was supported by the NSF of Guangdong Province (No.2022A1515011044, No.2023A1515010885), and the project of promoting research capabilities for key constructed disciplines in Guangdong Province (No.2021ZDJS028).

doscopy dataset covering 6 common nasal diseases as well as normal nasal samples; (2) We propose U-SEANNet, a novel lightweight U-architecture network. In addition, we added a new fusion module Global-Local Channel Feature Fusion inside it. It allows the network to make full use of the key channel features in the global and local feature maps, enabling U-SEANNet to accurately diagnose nasal endoscopic images while maintaining a lightweight; (3) We use five-fold cross-validation for the diagnostic performance of U-SEANNet is analyzed in detail and compared with 17 popular architectures including light-weight and heavy-weight networks.

2. FORMATTING YOUR PAPER

2.1. Data Source

The images used in this study were obtained from 20,000 patients who sought medical care in the Otolaryngology Department of Shenzhen University Second Affiliated Hospital from 2010 to 2020. All images were got by using standard endoscopes (Matrix E2, XION GmbH, Berlin, Germany) tethered to Olympus CV-170 digital endovision camera systems (Olympus Corporation, Tokyo, Japan). To ensure the accuracy of the labels, all images were cross-validated by four experts. During the screening process, each patient’s images were limited to a maximum of two. After removing images with inadequate quality and those that were difficult for experts to identify, a total of 11,527 images were collected, with the corresponding quantities for each disease class as follows: Rhinosinusitis (980, RHI), Nasopharyngeal Carcinoma (776, NC), Deviation of Nasal Septum (2338, DNS), Allergic Rhinitis (1122, AR), chronic rhinosinusitis with nasal polyps (1305, CRP), Adenoid Hypertrophy (1530, AH), and Normal (3476, Nor). All images were in JPG format with a size of 800×800×3 pixels. The research protocol of this study was approved by the Review Committee of the Second Affiliated Hospital of Shenzhen University (Approval No: BY-EC-SOP-006-01.0-A01). The Helsinki Declaration’s tenets were scrupulously followed throughout the study to respect the rights, privacy, and anonymity of the subjects. The use of de-identified data precluded the use of informed consent.

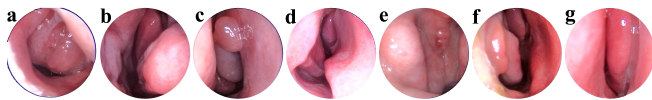


Fig. 1. The Samples of different types of nasal images. a. Adenoid Hypertrophy; b. Allergic Rhinitis; c. chronic rhinosinusitis with nasal polyps; d. Deviation of Nasal Septum. e. Nasopharyngeal Carcinoma; f. Normal; g. Rhinosinusitis.

2.2. Network Architecture

The overall framework of the model is shown in Figure 2. In details, at the beginning of the network, the Stem is respon-

sible for extracting initial features from the input image. It is comprised of a 3x3 convolution layer, batch normalization, and a ReLU6 activation function. Subsequently, a backbone composed of five Residual Shuffle Blocks, five MobileNetV2 blocks, and five Global-Local Channel Feature Fusion Modules further processes the extracted image features. Among these, the Shuffle residual block is responsible for extracting semantic information at different levels within the image. It does not alter the size of the feature map, and its internal structure is largely consistent with the blocks used in ShuffleNetV2. A slight difference is due to the smaller model capacity, we have additionally included a skip connection within it to enhance the model’s feature reuse. On the other hand, MobileNetV2 Block is tasked with performing down-sampling on the feature map and doubling the number of channels. Notably, the third MV2 Block only expands the channels, without performing down-sampling operations. Through the repeated stacking of Shuffle residual blocks and MV2 Blocks, efficient feature extraction is ensured, while maintaining the network’s lightweight characteristics. Additionally, to align the model with the computational precision issues on mobile devices, all activation functions within the backbone utilize the ReLU6 activation function. In the process of feature fusion, we concatenate shallow and deep feature maps along the channel dimension, and then apply ECA (Efficient Channel Attention) to guide the network to focus on key global and local features within the feature map. Subsequent point-wise convolutions ensure that global and local feature information can effectively flow across channels. Deep feature maps are also added to the final output, effectively boosting the network’s performance. At the end of the network, a traditional classifier is used to categorize the extracted image features. Given the uniqueness of our network, we have named it U-SEANNet.

2.3. Evaluation Metrics

Here, based on the characteristics of medical images, we have chosen to use Accuracy, Sensitivity, and Specificity as evaluation metrics for the model. The high or low values of these three metrics can reflect the potential of the model in disease diagnosis. Their calculation formulas are as follows:

$$Accuracy = \frac{TP + TN}{TP + TN + FP + FN}$$

$$Sensitivity = \frac{TP}{TP + FN}$$

$$Specificity = \frac{TN}{TN + FP}$$

In these equations, TP, TN, FP and FN are the numbers of true positives, true negatives, false positives and false negatives. In addition, we utilize GFLOPs and Parameters Size as metrics to evaluate whether the network meets the lightweight criteria.

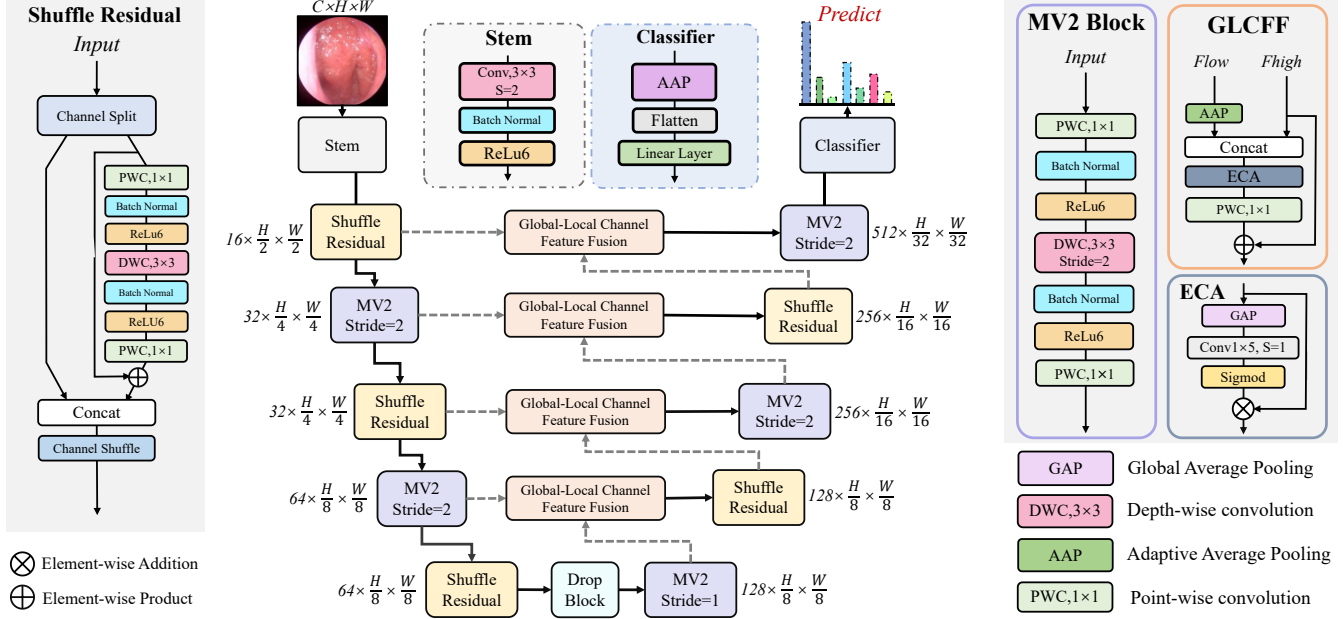


Fig. 2. The overall architecture of U-SEANNet. Here, MV2 refers to MobileNetV2 Block.

2.4. Implementation details

In this work, we adopted a five-fold cross-validation method to thoroughly evaluate the potential of our network. Specifically, the average value \pm standard deviation of the five-fold cross-validation results was used as the performance metric for the model. Before training the network, we resized all images to $224 \times 224 \times 3$. Subsequently, the images were normalized and standardized using the mean $[0.8398, 0.6, 0.6263]$ and standard deviation $[0.1849, 0.28, 0.2698]$ for the three channels. During the training process, we employed the Adam optimizer to optimize the model parameters, with a learning rate set to 0.001. Other parameters of the optimizer use the default configuration. We trained the model for 150 epochs, using a batch size of 128. To train the network, we utilized the PyTorch framework, and the training was conducted on a computer with Ubuntu 22.04 operating system and an NVIDIA GeForce RTX 4090 GPU.

3. RESULTS AND DISCUSSION

To prove the effectiveness of U-SEANNet, we chose six series of well-known networks, including both lightweight and heavyweight models, as reference models. These models are MobileNet[11, 12], EfficientNet[13], ResNet[14], DenseNet[15], MobileVit[16], and Swin Transformer[17]. Each of these models has its own advantages in the ImageNet classification task, and specific network names can be found in Table 1. Please note that the input image sizes for EfficientNet-B0 and EfficientNet-B1 are 240×240 and 260×260 , respectively, while the input size for the rest of the

networks is 224×224 . All models were trained strictly according to the requirements specified in the implementation details, and unified metrics were used for evaluation.

Table 1 presents the results of U-SEANNet and other networks in terms of Accuracy, GFLOPs, and Parameters Size. Regarding accuracy, among the selected reference networks, MobileNetV2, EfficientNet-B0, ResNet50, DenseNet201, MobileVit-XXS, and Swin Transformer-Tiny achieved the best performance within their respective families, with accuracies of 91.81%, 91.40%, 92.18%, 93.25%, 91.08%, and 90.80%, respectively. In contrast, our designed U-SEANNet achieved state-of-the-art results among all the networks, with an accuracy of 93.58%. Compared to the reference networks, U-SEANNet outperformed them by 1.77%, 2.18%, 1.40%, 0.33%, 2.50%, and 2.78% in accuracy, respectively. Meanwhile, U-SEANNet demonstrated the lowest GFLOPs and Parameters Size among all the networks, with values of only 0.21 and 0.78M, respectively. Compared to the heavyweight networks, such as ResNet50, DenseNet201, and Swin Transformer-Tiny, U-SEANNet achieved higher accuracy while significantly reducing GFLOPs by 94.9%, 95.2%, and 92.9%, and parameters size by only 3.3%, 4.3%, and 2.8% of their respective values. The experimental results clearly indicate that our work not only guarantees high accuracy in the network but also achieves remarkable lightweight characteristics, providing significant advantages for practical applications.

Next, in order to further analyze the potential of U-SEANNet in each disease diagnosis, we summarized the Sensitivity and Specificity of the networks for the 7 types of nasal images in Table 2. Additionally, we included the

Table 1. Accuracy, GFLOPs and Parameters Size of U-SEANNet and other reference networks.

Model	Accuracy	GFLOPs	Parameters Size
U-SEANNet	93.58%(±0.42)	0.21	0.78M
MobileNetV2	91.81%(±0.67)	0.32	2.23M
MobileNetV3-Large	91.79%(±0.58)	0.23	4.21M
EfficientNet-B0	91.40%(±0.21)	0.4	4.02M
EfficientNet-B1	90.88%(±0.23)	0.71	6.52M
EfficientNet-B2	90.89%(±0.48)	1.03	7.71M
ResNet50	92.18%(±0.40)	4.12	23.52M
ResNet101	92.01%(±0.31)	7.84	42.51M
ResNet152	91.76%(±0.51)	11.57	58.16M
DenseNet121	93.24%(±0.43)	2.88	6.96M
DenseNet161	92.97%(±0.40)	7.82	26.49M
DenseNet201	93.25%(±0.45)	4.37	18.11M
MobileVit-S	81.96%(±2.43)	1.44	4.94M
MobileVit-XS	90.85%(±0.40)	0.72	1.94M
MobileVit-XXS	91.08%(±0.22)	0.26	0.95M
SwinTransformer-T	90.80%(±0.54)	2.97	27.52M
SwinTransformer-S	90.11%(±0.51)	5.75	48.84M
SwinTransformer-B	89.15%(±0.29)	10.21	86.75M

results of the best-performing network from each family for reference. As shown in Table 2, U-SEANNet achieved the highest Sensitivity in four categories: AR, DNS, NC, and RHI, with respective scores of 77.28%, 93.93%, 99.87%, and 96.74%. At the same time, U-SEANNet achieved the best performance in Specificity for the AH, CRP, NOR, and RHI categories, with results of 99.81%, 99.42%, 96.68%, and 99.39%, respectively.

The experimental results demonstrate that, through a comprehensive analysis of Accuracy, GFLOPs, Parameters Size, Sensitivity, and Specificity, our work not only facilitates convenient application on practical devices but also exhibits the best potential for diagnosing nasal diseases.

4. CONCLUSION

This paper introduces a simple, efficient and applied network for diagnosing nasal diseases. Our network not only surpasses state-of-the-art neural networks in terms of Accuracy but also exhibits extremely low GFLOPs and Parameters Size. Our next step in this research is to address the issue of imbalanced datasets. It is evident that due to the presence of class imbalances, the diagnostic capabilities for the AR and CRP diseases are slightly insufficient. Additionally, we will conduct further testing of the model on diverse populations and develop specific applications accordingly. Furthermore, we plan to explore the feasibility of conducting human-machine comparative studies, which help in evaluating how the model performs in real-world scenarios with the involvement of human expertise, enhancing its overall utility and applicability.

Table 2. The Sensitivity of U-SEANNet and other networks for the seven types of diseases.

Model	Diseases	Sensitivity	Specificity
U-SEANNet	AH	98.23%(±0.67)	98.23%(±0.67)
	AR	77.28%(±3.25)	77.28%(±3.25)
	CRP	92.18%(±0.90)	92.18%(±0.90)
	DNS	93.93%(±1.00)	93.93%(±1.00)
	NC	99.87%(±0.26)	99.87%(±0.26)
	NOR	94.79%(±1.01)	94.79%(±1.01)
	RHI	96.74%(±1.39)	96.74%(±1.39)
MobileNetV2	AH	98.23%(±0.67)	98.23%(±0.67)
	AR	77.28%(±3.25)	77.28%(±3.25)
	CRP	92.18%(±0.90)	92.18%(±0.90)
	DNS	93.93%(±1.00)	93.93%(±1.00)
	NC	99.87%(±0.26)	99.87%(±0.26)
	NOR	94.79%(±1.01)	94.79%(±1.01)
	RHI	96.74%(±1.39)	96.74%(±1.39)
EfficientNet-B0	AH	98.23%(±0.67)	98.23%(±0.67)
	AR	77.28%(±3.25)	77.28%(±3.25)
	CRP	92.18%(±0.90)	92.18%(±0.90)
	DNS	93.93%(±1.00)	93.93%(±1.00)
	NC	99.87%(±0.26)	99.87%(±0.26)
	NOR	94.79%(±1.01)	94.79%(±1.01)
	RHI	96.74%(±1.39)	96.74%(±1.39)
ResNet50	AH	98.23%(±0.67)	98.23%(±0.67)
	AR	77.28%(±3.25)	77.28%(±3.25)
	CRP	92.18%(±0.90)	92.18%(±0.90)
	DNS	93.93%(±1.00)	93.93%(±1.00)
	NC	99.87%(±0.26)	99.87%(±0.26)
	NOR	94.79%(±1.01)	94.79%(±1.01)
	RHI	96.74%(±1.39)	96.74%(±1.39)
DenseNet201	AH	98.23%(±0.67)	98.23%(±0.67)
	AR	77.28%(±3.25)	77.28%(±3.25)
	CRP	92.18%(±0.90)	92.18%(±0.90)
	DNS	93.93%(±1.00)	93.93%(±1.00)
	NC	99.87%(±0.26)	99.87%(±0.26)
	NOR	94.79%(±1.01)	94.79%(±1.01)
	RHI	96.74%(±1.39)	96.74%(±1.39)
MobileVit-XXS	AH	98.23%(±0.67)	98.23%(±0.67)
	AR	77.28%(±3.25)	77.28%(±3.25)
	CRP	92.18%(±0.90)	92.18%(±0.90)
	DNS	93.93%(±1.00)	93.93%(±1.00)
	NC	99.87%(±0.26)	99.87%(±0.26)
	NOR	94.79%(±1.01)	94.79%(±1.01)
	RHI	96.74%(±1.39)	96.74%(±1.39)
SwinT-T	AH	98.23%(±0.67)	98.23%(±0.67)
	AR	77.28%(±3.25)	77.28%(±3.25)
	CRP	92.18%(±0.90)	92.18%(±0.90)
	DNS	93.93%(±1.00)	93.93%(±1.00)
	NC	99.87%(±0.26)	99.87%(±0.26)
	NOR	94.79%(±1.01)	94.79%(±1.01)
	RHI	96.74%(±1.39)	96.74%(±1.39)

5. REFERENCES

- [1] Wen Wen, Shi-Juan Mai, Huan-Xin Lin, Mei-Yin Zhang, Jia-Ling Huang, Xin Hua, Chao Lin, Zhi-Qing Long, Zi-Jian Lu, Xiao-Qing Sun, et al., “Identification of two microrna signatures in whole blood as novel biomarkers for diagnosis of nasopharyngeal carcinoma,” *Journal of translational medicine*, vol. 17, pp. 1–13, 2019.
- [2] Carla Mastrorilli, Daniela Posa, Francesca Cipriani, and Carlo Caffarelli, “Asthma and allergic rhinitis in childhood: what’s new,” *Pediatric Allergy and Immunology*, vol. 27, no. 8, pp. 795–803, 2016.
- [3] Fuad M Baroody, “Allergic rhinitis: broader disease effects and implications for management,” *Otolaryngology—Head and Neck Surgery*, vol. 128, no. 5, pp. 616–631, 2003.
- [4] Benton Girdler, Hyun Moon, Mi Rye Bae, Sung Seok Ryu, Jihye Bae, and Myeong Sang Yu, “Feasibility of a deep learning-based algorithm for automated detection and classification of nasal polyps and inverted papillomas on nasal endoscopic images,” in *International Forum of Allergy & Rhinology*. Wiley Online Library, 2021, vol. 11, pp. 1637–1646.
- [5] Y K Maru and Y Gupta, “Nasal endoscopy versus other diagnostic tools in sinonasal diseases,” *Indian Journal of Otolaryngology and Head & Neck Surgery*, vol. 68, pp. 202–206, 2016.
- [6] Utku Aydil, Hande Karadeniz, and Caner Şahin, “Choanal polyp originated from the inferior nasal concha,” *European archives of oto-rhino-laryngology*, vol. 265, no. 4, pp. 477–479, 2008.
- [7] Xinyu Zeng, Zifan Jiang, Wen Luo, Honggui Li, Hongye Li, Guo Li, Jingyong Shi, Kangjie Wu, Tong Liu, Xing Lin, et al., “Efficient and accurate identification of ear diseases using an ensemble deep learning model,” *Scientific Reports*, vol. 11, no. 1, pp. 10839, 2021.
- [8] Zhenzhen You, Yan Yan, Zhenghao Shi, Minghua Zhao, Jing Yan, Haiqin Liu, Xinhong Hei, and Xiaoyong Ren, “Laryngeal leukoplakia classification via dense multi-scale feature extraction in white light endoscopy images,” in *ICASSP 2023-2023 IEEE International Conference on Acoustics, Speech and Signal Processing (ICASSP)*. IEEE, 2023, pp. 1–5.
- [9] Ramanuj Bhattacharjee, K Suganya Devi, and S Vijaykanth, “Detecting laryngeal cancer lesions from endoscopy images using deep ensemble model,” in *2023 International Conference on Signal Processing, Computation, Electronics, Power and Telecommunication (IConSCEPT)*. IEEE, 2023, pp. 1–6.
- [10] Mingmin Bi, Siting Zheng, Xuechen Li, Haiyan Liu, Xiaoshan Feng, Yunping Fan, and Linlin Shen, “Mib-anet: A novel multi-scale deep network for nasal endoscopy-based adenoid hypertrophy grading,” *Frontiers in Medicine*, vol. 10, pp. 1142261, 2023.
- [11] Andrew G Howard, Menglong Zhu, Bo Chen, Dmitry Kalenichenko, Weijun Wang, Tobias Weyand, Marco Andreetto, and Hartwig Adam, “Mobilenets: Efficient convolutional neural networks for mobile vision applications,” *arXiv preprint arXiv:1704.04861*, 2017.
- [12] Andrew Howard, Mark Sandler, Grace Chu, Liang-Chieh Chen, Bo Chen, Mingxing Tan, Weijun Wang, Yukun Zhu, Ruoming Pang, Vijay Vasudevan, et al., “Searching for mobilenetv3,” in *Proceedings of the IEEE/CVF international conference on computer vision*, 2019, pp. 1314–1324.
- [13] Mingxing Tan and Quoc Le, “Efficientnet: Rethinking model scaling for convolutional neural networks,” in *International conference on machine learning*. PMLR, 2019, pp. 6105–6114.
- [14] Kaiming He, Xiangyu Zhang, Shaoqing Ren, and Jian Sun, “Deep residual learning for image recognition,” in *Proceedings of the IEEE conference on computer vision and pattern recognition*, 2016, pp. 770–778.
- [15] Gao Huang, Zhuang Liu, Laurens Van Der Maaten, and Kilian Q Weinberger, “Densely connected convolutional networks,” in *Proceedings of the IEEE conference on computer vision and pattern recognition*, 2017, pp. 4700–4708.
- [16] Sachin Mehta and Mohammad Rastegari, “Mobilevit: light-weight, general-purpose, and mobile-friendly vision transformer,” *arXiv preprint arXiv:2110.02178*, 2021.
- [17] Ze Liu, Yutong Lin, Yue Cao, Han Hu, Yixuan Wei, Zheng Zhang, Stephen Lin, and Baining Guo, “Swin transformer: Hierarchical vision transformer using shifted windows,” in *Proceedings of the IEEE/CVF international conference on computer vision*, 2021, pp. 10012–10022.